# Alternative PF coil winding pack design for the EU DEMO

M. Kumar, R. Guarino, K. Sedlak, X. Sarasola, and P. Bruzzone

***Abstract*— The EUROfusion DEMO machine is at its pre-conceptual stage. The design of the magnet system for this machine is being developed in collaboration with several European research centers. The Poloidal Field (PF) coils proposed by the Swiss Plasma Center (SPC) use a multiple-in-hand Pancake winding technique. A design based on updated plasma scenarios (2018) was recently proposed. The Winding Pack (WP) aspect ratio was kept close to one, similar to the baseline design in the EUROfusion 2018 DEMO baseline document. In this publication, we study the effects of changing WP aspect ratio. A vertically elongated WP cross-section is beneficial in the reduction of the peak magnetic field at WP cross-section, the machine radial extent, and the hydraulic lengths. However, it increases the bending stress on the WP. An updated PF design is presented. The dimensioning and allocation of materials is based on 3-dimensional electromagnetic calculations. Mechanical performance is evaluated against both dynamic fatigue stress and static stresses. The static stresses are evaluated through 3-dimensional finite element simulations to take into account also the ripple effect of TF coils and increase in bending stresses due to the elongation of the WP cross-section. The thermal-hydraulic analysis verifies a temperature margin of 1.5 K and confirms sufficient coolant flow for the prescribed pressure drop. The quench analysis determines the hot-spot temperatures during various quench scenarios.**

***Index Terms*—Fusion, DEMO, Superconducting magnets, PF coil, CIC forced flow cable.**

## I. Introduction

The EUROfusion DEMO pulsed tokamak fusion reactor is currently at the pre-conceptual design stage. The magnet system of this reactor is mostly based on Low-Temperature Superconductors (LTS). The Poloidal Field (PF) coils of this magnet system are being developed in the framework of EUROfusion Work Package MAGnets (WPMAG) at several European research centers [1] [2].

All six PF coils (PF1 to PF6) are designed as rectangular cross-section Winding Packs (WP). The design proposed by the Swiss Plasma Center (SPC) in 2018 satisfied the 19.6 MA plasma current scenario [3]. In 2019, a preliminary design was proposed for the newly available 17.86 MA plasma current scenario [4]. The design was based on coil currents in three different plasma states: Premagnetisation (PREMAG), Start Of Flattop (SOF), and End Of Flattop (EOF). This updated design used the pancake winding technique instead of the layer winding technique for the PF magnet system because pancake winding facilitates easier cable handling during winding at large radii. Due to the large currents and field in PF1 and PF6 coils, $Nb_3Sn$ was used as a superconductor in these two coils instead of NbTi, consequently reducing the WP cross-section significantly. This work only dealt with pre-designing of the WP and allocating the materials without the thermal-hydraulic and quench analysis, and without a 3-dimensional mechanical analysis.

In the present work, we propose an updated Winding Pack (WP) layout for each of the six PF coils (PF1–PF6) based on, 1) the electromagnetic calculations in 3-dimensional geometry to optimize parameters such as effective magnetic field, coil inductances, and dump voltages, 2) the thermal-hydraulic and quench analyses to verify sufficient flow for given pressure drop, ensure 1.5 K temperature margin in normal operation and verify the hot-spot temperatures are within the prescribed limit, 3) detailed 3-dimensional mechanical analysis followed by dynamic fatigue stress analysis to verify whether the structure withstands static and dynamic mechanical loads. The aspect ratio of the WPs are varied to 1) reduce the peak field on WP and 2) decrease the hydraulic length of the conductor. The reduction in peak magnetic field on the WP allows using the NbTi superconductor also for the PF1 and PF6 coils [5]. However, elongating the WP cross-sections increase bending stresses in the coils leading to an increase in the required amount of steel in the conductor jacket.

This paper is organized as follows. Section II describes the overall design and methodology. The results are presented and discussed in Section III. In the end, we discuss the advantages and disadvantages of the proposed design and future outlook.

## II. Design Assumptions and Methodologies

All PF Coils are made with the Double Pancakes (DP), wound with 2-in-hand technique. The design of the conductor is well described in previous publications [3], [4]. The NbTi-based rectangular Cable-In-Conduit Conductor (CICC) has a 316LN stainless steel jacket with stadium shaped inner cable space and carries current in the range from 50-60 kA[3]. It has no separated low impedance cooling channel for manufacturing

This work has been carried out within the framework of the EUROfusion Consortium and has received funding from the Euratom research and training programme 2014-2018 and 2019-2020 under grant agreement No 633053. The views and opinions expressed herein do not necessarily reflect those of the European Commission. (*Corresponding author: Mithlesh Kumar)*

M. Kumar, R. Guarino, K. Sedlak, X. Sarasola and P. Bruzzone are with École Polytechnique Fédérale de Lausanne (EPFL), Swiss Plasma Center (SPC), CH-5232 Villigen PSI, Switzerland (e-mail: mithlesh.kumar@psi.ch).

Color versions of one or more of the figures in this paper are available online at http://ieeexplore.ieee.org.

Digital Object Identifier will be inserted here upon acceptance.

Template version 8.0d, 22 August 2017. IEEE will put copyright information in this area
See http://www.ieee.org/publications_standards/publications/rights/index.html for more information.

TABLE I
WINDING PACK GEOMETRY

| Coil | $R$ (m) | WP $dZ$ (mm) | WP $dR$ (mm) | Cond $dZ$ (mm) | Cond $dR$ (mm) | Jacket d$x$ (mm) |
|---|---|---|---|---|---|---|
| PF1 | 5.6 | 1760.0 | 701.4 | 75.3 | 50.6 | 10 |
| PF2 | 13.8 | 675.0 | 539.2 | 61.9 | 50.1 | 11 |
| PF3 | 17.7 | 1240.0 | 496.0 | 72.5 | 51.1 | 13 |
| PF4 | 17.7 | 1400.0 | 558.9 | 65.2 | 47.2 | 10 |
| PF5 | 13.8 | 890.0 | 711.3 | 68.8 | 47.5 | 11 |
| PF6 | 7.2 | 2260.0 | 911.1 | 76.1 | 57.5 | 9.5 |

TABLE II
CONDUCTOR LAYOUT AND ELECTROMAGNETIC PARAMETERS

| Coil | $I_{max}$ (MA) | $N_P$ | $N_L$ | $B_{eff}$ (T) | $L$ (H) | $V_{dump}$ (kV) | $WP$ AR |
|---|---|---|---|---|---|---|---|
| PF1 | 16.5 | 22 | 13 | 6.22 | 1.40 | 5.4 | 0.4 |
| PF2 | 5.9 | 10 | 10 | 4.51 | 0.69 | 2.7 | 0.8 |
| PF3 | 8.5 | 16 | 9 | 5.03 | 1.77 | 6.9 | 0.4 |
| PF4 | 12.0 | 20 | 11 | 5.71 | 3.98 | 14.5 | 0.4 |
| PF5 | 9.9 | 12 | 14 | 5.21 | 1.81 | 7.1 | 0.8 |
| PF6 | 24.0 | 28 | 15 | 6.34 | 3.86 | 14.7 | 0.4 |

TABLE III
STRESSES IN CONDUCTOR JACKET AND CORRESPONDING LIMITING STATES

| Coil | $\sigma_{hoop}$ (MPa) Avg | $\sigma_{hoop}$ (MPa) Max | Cycles until break ($x10^3$) | $\sigma_{hoop}$ limit (MPa) | Limiting current state |
|---|---|---|---|---|---|
| PF1 | 194 | 216 | 67.4 | 339 | PREMAG |
| PF2 | 184 | 257 | 58.0 | 339 | EOF |
| PF3 | 77 | 230 | 68.9 | 357 | PREMAG |
| PF4 | 112 | 231 | 56.4 | 330 | PREMAG |
| PF5 | 190 | 253 | 47.6 | 339 | EOF |
| PF6 | 178 | 207 | 71.0 | 330 | PREMAG |

TABLE IV
TEMPERATURE MARGIN AND HOT SPOT TEMPERATURES IN COILS.

| Coil | $L_{hyd}$ (m) | $\dot{m}$ (g/s) | $[\theta_{marg}]_{min}$ (K) | $MQE$ (J) | $\theta_{hotspot}$ Strand (K) | $\theta_{hotspot}$ Jacket (K) |
|---|---|---|---|---|---|---|
| PF1 | 212 | 16.5 | 1.56 | 41 | 54.6 | 49.2 |
| PF2 | 434 | 7.1 | 1.54 | 24 | 62.9 | 54.5 |
| PF3 | 444 | 7.3 | 1.53 | 24 | 58.6 | 49.3 |
| PF4 | 557 | 6.9 | 1.52 | 17.5 | 58.8 | 51.6 |
| PF5 | 605 | 6.1 | 1.54 | 18 | 59.9 | 51.7 |
| PF6 | 318 | 17.5 | 1.54 | 57 | 43.0 | 40.5 |

TABLE V
COMPARISON OF OLD DESIGN WITH NEW DESIGN.

| Coil | $AR$ Old | $AR$ New | $B_{eff}$(T) Old | $B_{eff}$(T) New | $WP\ area$(m$^2$) Old | $WP\ area$(m$^2$) New | $L_{hyd}$ (m) Old | $L_{hyd}$ (m) New |
|---|---|---|---|---|---|---|---|---|
| PF1 | 1.00 | 0.40 | 7.99 | 6.22 | 1.00 | 1.23 | 339 | 229 |
| PF2 | 0.83 | 0.80 | 4.68 | 4.51 | 0.33 | 0.36 | 434 | 434 |
| PF3 | 0.78 | 0.40 | 5.85 | 5.03 | 0.43 | 0.61 | 667 | 499 |
| PF4 | 1.00 | 0.40 | 6.14 | 5.71 | 0.67 | 0.78 | 952 | 611 |
| PF5 | 1.00 | 0.80 | 5.43 | 5.21 | 0.59 | 0.63 | 649 | 605 |
| PF6 | 1.00 | 0.40 | 9.00 | 6.34 | 1.45 | 2.06 | 505 | 341 |

simplicity. The high void fraction (40%) allows sufficient Helium flow through the cable bundle [6], [7]. Feeders in the ITER magnet system are designed on the same concept [8]. Copper to non-copper ratio (Cu/Non-Cu) is set equal to 1.3 for all superconducting strands. In the previously proposed design, it was set equal to 1. The increase in Cu/non-Cu comes from the manufacturing limit for NbTi strands for PF coils. Target current density in copper is 105 A/mm$^2$. A rectangular cable with a steel strip in the mid-plane is attractive to lower AC losses.

The electrical insulation scheme is described in the previous publication [4] except that we removed the turn shim because the turn to turn voltages are very low when compared to the pancake to pancake voltages. The allocation of materials is based on the analyses presented in the following subsections.

### *A. Electromagnetic analyses methodology*

Methodology for electromagnetic calculations and evaluation of parameters are already described in the previous publications [3], [4]. The whole 3-dimensional geometry of the magnet system is divided using elementary current-carrying bricks in the MC module of Cryosoft. The magnetic fields are then calculated at the points of interest using superposition. The plasma is modeled as a circular coil at the plasma center.

### *B. Mechanical analyses Methodology*

Static stresses are calculated using 3-dimensional Finite Element (FE) simulations in ANSYS with homogenized thermo-mechanical properties, extracted as described in [9]. All the three plasma current states are simulated and the thermal stresses due to cool down from room temperature to 4.5 K are also included. The resulting hoop stresses in the jacket are used iteratively as inputs in fatigue stress analyses, which determine the limiting values and whose details can be found in [4] and [10]. The procedure is illustrated in Fig. 1. The safety factors recommended by ITER was used [11]. The fatigue analysis makes use of a simple crack growth model based on Linear Elastic Fracture Mechanics (LEFM). This model uses Paris law to grow a planar elliptical crack across the thickness of a 2D plate with the width and thickness of the conduit wall. The model is described in [10], which in turn is based on the method and recommendations of ITER Magnet Structural Design Criteria [11]. The dimensions of the embedded and surface cracks are 5mm$^2$ and 2mm$^2$ respectively.

### *C. Thermal-hydraulic analyses methodology*

The thermal-hydraulic calculations are performed on conductors of all the PF coils using the current scenario shown in Fig.2. The coolant inlet is located at the pancake transition on the inner side in each DP, while the outlet is on the outer side of the pancake. The heat deposition due to AC coupling loss per unit length of the conductor is calculated as

$$P_{coupling}(x) = \frac{n\tau S}{\mu_0}\left(\frac{d\vec{B}(x)}{dt}\right)^2$$

The coupling loss time constant for PF conductors is assumed to be $n\tau$ =150 ms [7]. $S$ is the area of superconducting strands and segregated copper strands in the conductor cross-section. The heat deposition due to nuclear heat load, hysteresis losses, eddy current losses, etc. are neglected at the pre-conceptual design phase. The justification is given in this reference [7].

The thermal-hydraulic model is shown in Fig.3. The magnetic field along the conductor length is assumed constant and equal to the maximum $B_{eff}$ value for the respective coil. Helium flows in the bundle region inside the cable space. The darcy-

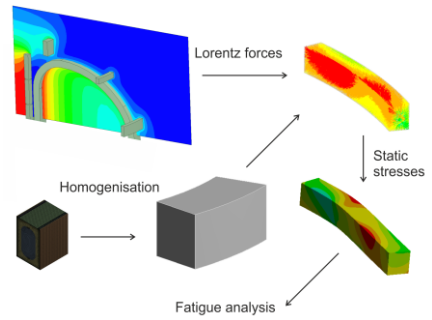


Fig. 1. Procedure for Mechanical analyses.

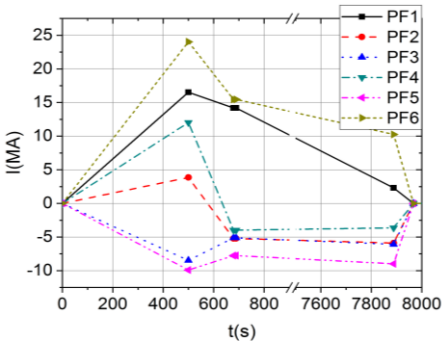


Fig. 2. Total Current evolution in PF coils.

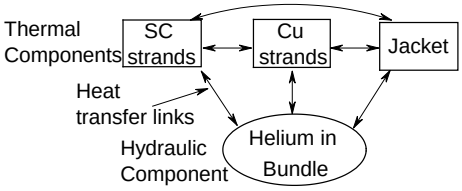


Fig.3 Thermal-hydraulics model used in calculations.

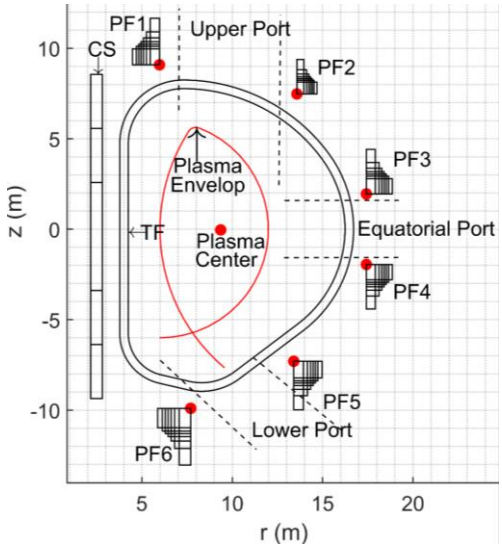


Fig.4 Vertical cross-section of the magnet system. Red dots are kept fixed while varying the AR of WP.

Forchheimer equation is used for friction factor correlation. Dittus-Boelter correlation is used for heat transfer correlation. The inlet helium pressure is 6 bar and the temperature is 4.5 K, while the outlet pressure is 5 bar. Inter-turn (IT) and inter-layer (IL) heat transfer was not considered. The adiabatic assumption is indeed conservative. The hot-spot temperature of the jacket for the case without IT is typically (0.6 – 8 K) higher than for the case with IT [12].

The duration of each plasma cycle is 8067 s. The temperature margin is calculated as the difference between the strand current sharing temperature $\theta_{CS}(x,t)$ and the strand temperature $\theta(x,t)$: $\theta_{margin} = \theta_{CS}(x,t) - \theta(x,t)$. The $\theta_{margin}$ attained periodicity with time at the end of the second pulse. Quench is initiated at 100 m from the inlet by a heat pulse over the length of 10 cm and duration 100 ms, and Quench Initiation Energy, *QIE* = 2 x *MQE* (Minimum Quench Energy). *MQE* is evaluated iteratively. The quench detection voltage threshold was set at 0.1 V. The current dump, assumed exponential with a characteristic time $\tau_{dump}$ = 15 s, starts with an additional delay of 1.1 s corresponding to the quench protection system reaction time. During the fast discharge, the magnetic field decreases proportionally to the operating current, which induces heat generation.

## III. Results and Discussion

The final conductor dimensions and WP layouts were obtained after several iterations of electromagnetic, mechanical, and thermal-hydraulics analyses. We studied a broad range of aspect ratios (AR) of WP cross-section as shown in Fig. 4. The choice of AR depends on several factors. For PF1 and PF6 coils, a decrease in aspect ratio AR (defined as the ratio of radial to the vertical dimension of WP cross-section) causes a decrease in the peak field at the coil, hoop stress (excluding bending moments), and conductor hydraulic length. It also provides more vertical space for the upper ports and the pellet fuel injection line. On the other hand, the overall hoop stress increases due to an increase in bending moment, and the centerline of WP also moves away from the plasma center. For PF6 coils, a vertical elongation elevates the whole Tokamak. The $B_{eff}$ on PF2 coil WP is the smallest. The advantage of WP elongation is therefore insignificant. For PF3 and PF4 coils, a decrease in AR causes a decrease in peak magnetic field on the coil, hydraulic length, and radial extent of these coils. This means that the radius of the cryostat and bio-shield is decreased. Decreasing AR of these coils also allows the port duct and therefore the equatorial port vacuum closure plate to be moved closer to the plasma. For the PF5 coil, the AR cannot be decreased significantly due to its location near the lower port (see Fig. 4).

Finally, we chose AR as given in table II. The proposed design and electromagnetic parameters are given in Table I and II. The abbreviation used is dZ for vertical dimension, dR for radial dimension, Cond for Conductor, $I_{MAX}$ for coil maximum total current, $N_P$ and $N_L$ for the number of pancakes and number of turns per pancake respectively, $B_{eff}$ for the effective magnetic field, L for coil self-inductance, $V_{dump}$ for the maximum terminal to terminal voltage and dx stands for conductor jacket thickness. The diameters of the NbTi superconducting strands and the segregated copper strands are set to 0.8mm. For PF1-PF6 coils, the number of superconducting strands are 1919, 280, 405, 756, 480, and 2527 respectively. The number of segregated copper strands are 0, 960, 890, 609, 855, and 0 respectively. All the coils with an AR = 0.4 are elongated in the vertical direction. This could be challenging for the coil integration with the

whole reactor system. On the other hand, all the coils have a smaller extent in the radial direction, thus reducing the reactor radial dimension. The vertical dimension of the conductor for PF1 and PF6 coils are also greater than 75 mm. A conductor sample of such dimensions will be challenging to test in the bore of the SULTAN test facility [12]. We could decrease conductor dZ and increase dR, but then we would lose the advantages of a rectangular conductor. Moreover, a design based on a square conductor has already been proposed [5].

The results of mechanical analyses are given in Table III. The fatigue is the main driver for the structural design of the PF coils. The 3-dimensional analyses allow considering the ripples in the magnetic fields generated by the TF coils. This extra field increases the bending moment on the PF, consequently increasing the hoop stress ($\sigma_{hoop}$). The limiting value of $\sigma_{hoop}$ (corresponding to 20000 plasma cycles) is found through the fatigue stress analysis. We found that the case of embedded cracks is systematically more conservative than the case of surface cracks. For PF5 coil, the maximum total current is seen in PREMAG state, but the maximum hoop stress is seen by the conductor jacket in the EOF state. This derives from the contribution to the magnetic fields generated by the other coils. The obtained values of the number of cycles until break listed in Table III suggest a slightly overdesigned jacket thickness. A further reduction of the jacket thickness was also considered, but it leads to the concentration of stress in some locations.

The results of thermal-hydraulic analyses are given in Table IV. The abbreviation used is $L_{hyd}$ for conductor hydraulic length, $\dot{m}$ for mass flow rate, and $\theta$ for temperature. The profiles of temperature distribution along conductor length and their evolution with time during normal operation and conductor quench were obtained. Temperature margins during normal operation and the maximum values (in space and time) of the bundle strands and jacket temperatures obtained in the quench simulations are given in this table. We notice that $\theta_{margin}$ >1.5 K for all the PF coils. In the PF conductors, the hot-spot temperature acceptance criterion is $\theta_{hotspot}$ < 150 K for the jacket and $\theta_{hotspot}$ < 250 K for the strands [14]. The table shows that indeed $\theta_{hotspot}$ is much smaller than the limiting value. This is due to a large amount of copper in the conductor cross-section and it hints towards an over-conservative design for the amount of copper. A simplified calculation was done to verify this result. We assumed that after quench all the current flows through copper in the conductor, which results in joule heating. Assuming, 1) that the temperature of copper in the conductor is allowed to rise adiabatically in the absence of other materials in the conductor and 2) that the normal zone propagation velocity is infinite, the temperature of copper is given by

$$\theta(t) = \int_0^t [I^2_{conductor}(t)\, R_{Cu}(t)/m_{Cu}\, C(t)]dt$$

Here, $R_{Cu}$ is temperature and magnetic field dependent resistance of copper, $m_{Cu}$ is mass of copper and $C$ is the temperature-dependent specific heat of copper. The asymptotic value of $\theta$ for all PF conductors is found always less than 120 K. This supports the conclusion about a slightly overestimated amount of copper.

As given in Table V, when compared to the design proposed last year [4], the effect of aspect ratio change on $B_{eff}$ is only marginal. But for PF1 and PF6 coils, the reduction in $B_{eff}$, allows the use of NbTi in the conductor. However, compared to the $Nb_3Sn$ conductor based design for PF1 and PF6 coils, the proposed coils are much bigger. The WP areas have increased in the newly proposed design even though $B_{eff}$ is reduced. This is due to an increased amount of steel in the new design. Previously, the design was based on mechanical analyses in a 2-dimensional axisymmetric geometry. Possibly, the amount of steel in the jacket was underestimated. The jacket thicknesses in the older design for PF1 to PF6 coils were 10.5, 9, 6, 6, 9, 10.5 mm respectively; while the same in the new design are 10, 11, 13, 10, 11, 9.5 mm respectively. Due to the smaller radial extent of WPs, the conductor hydraulic lengths have decreased significantly for all the coils, except for PF2 and PF5 coils for which AR has not changed significantly. The change in AR causes magnetic field variation at the plasma center and the plasma envelop within ±3%.

## IV. Conclusion

The proposed design of EU DEMO PF coils has a low WP cross-section aspect ratio. The aspect ratio for each coil is decided based on several geometrical and some limiting physical parameters. The reduction in peak magnetic field at PF1 and PF6 coils allows using the NbTi superconductor. However, the resulting WP is huge in the vertical direction and could be challenging for the coil integration in the whole machine. The dimensions of conductors for these coils are also larger than currently testable conductors in the SULTAN test facility. To solve this problem, conductor current could be reduced but it would lead to a higher number of turns and hence higher self-inductance and dump voltage. We can also reduce the jacket thickness of the test conductor for testing in SULTAN bore. Another solution could be to use the $Nb_3Sn$ superconductor for these coils as proposed in the previous work [4]. This would not only help to reduce the conductor dimension but also the overall WP dimension in the vertical direction and consequently it would also ease integration issues of these coils with the whole machine. The amount of steel is again limited by fatigue rather than static stresses. The thermal-hydraulic analyses showed that the proposed conductors respect the 1.5 K temperature margin limit. The quench analyses showed a large margin in terms of hot spot temperature. To reduce the amount of copper in PF2 to PF5 coils, the assumed current density in copper could be increased parametrically until the limiting value of hotspot temperature is reached. In PF1 and PF6, due to a large number of superconducting strands, the amount of copper is limited by the Cu/non-Cu ratio (1.3 is the lowest value for manufacturability of NbTi strands). Another solution is to use the $Nb_3Sn$ superconductor to reduce the required number of strands drastically. However, $Nb_3Sn$ based conductor requires heat treatment and careful cable handling, thus adding to manufacturing complexity and costs. The trade-off in material cost, manufacturing and assembly related costs and risks for both NbTi and $Nb_3Sn$ variants needs to be carefully assessed.

## REFERENCES


[1] V. Corato *et al*., "Progress in the design of the superconducting magnets for the EU DEMO," Fusion Engineering and Design, vol. 136, pp. 1597-1604, 2018.

[2] K. Sedlak *et al.*, "Advance in the conceptual design of the European DEMO magnet system", Superconductor Science and Technology, vol. 33, 044013, 2020.

[3] M. Kumar *et al*., "Design of DEMO PF Coils Based on Cable-in-Conduit Conductor." IEEE Transactions on Applied Superconductivity, vol. 29, no. 5, pp. 1-4, 2019.

[4] M. Kumar *et al*., "Preliminary design of DEMO PF coils based on EU DEMO 2018 baseline." IEEE Transactions on Applied Superconductivity, vol. 30, no. 4, pp. 1-5, 2020.

[5] L. Zani *et al*., "CEA Broad Studies on EU DEMO CS and PF Magnet Systems," in IEEE Transactions on Applied Superconductivity, vol. 30, no. 4, pp. 1-6, June 2020.

[6] K. Hamada *et al.*, "Effect of electromagnetic force on the pressure drop and coupling loss of a cable-in-conduit conductor," Cryogenics, vol. 44, no. 1, pp. 45-52, 2004.

[7] A. Zappatore *et al*., "Performance analysis of the NbTi PF coils for the EU DEMO fusion reactor," IEEE Transactions on Applied Superconductivity, vol. 28, no. 4, pp. 1-5, 2018.

[8] M. Calvi, *et al.*, "Design Proposal for the ITER Feeder Busbars," in IEEE Transactions on Applied Superconductivity, vol. 20, no. 3, pp. 407-410, June 2010.

[9] F. Nunio *et al.*, "Reference basis for mechanical & thermal analysis of TFC", 10 March 2015, https://idm.euro-fusion.org/?uid=2MC8T4.

[10] X. Sarasola *et al.*, "Progress in the Design of a Hybrid HTS-Nb3Sn-NbTi Central Solenoid for the EU DEMO," in IEEE Transactions on Applied Superconductivity, vol. 30, no. 4, pp. 1-5, June 2020.

[11] C. Jong, "Magnet Structural Design Criteria Part 1: Main Structural Components and Welds," ITER, UID: 2FMHHS.

[12] A. Dembkowska, M. Lewandowska and X. Sarasola, "Thermal-Hydraulic Analysis of the DEMO CS Coil," in IEEE Transactions on Applied Superconductivity, vol. 28, no. 4, pp. 1-5, June 2018.

[13] P. Bruzzone et al., "Upgrade of operating range for SULTAN test facility," in IEEE Transactions on Applied Superconductivity, vol. 12, no. 1, pp. 520-523, March 2002.

[14] K. Sedlak, "DEMO Magnet Design Philosophy Manual", June 2020, https://idm.euro-fusion.org/?uid=2NWKYS.